JoT JOURNAL OF TURBULENCE

http://jot.iop.org/

The relationship between mean and instantaneous structure in turbulent passive scalar plumes†

John P Crimaldi[1], Megan B Wiley[2] and Jeffrey R Koseff[2]

[1] Department of Civil and Environmental Engineering, University of Colorado, 428 UCB, Boulder, CO 80309-0428, USA
[2] Department of Civil and Environmental Engineering, Stanford University, Stanford, CA 94305-4020, USA
E-mail: john.crimaldi@colorado.edu

Received 3 December 2001
Published 4 March 2002

Abstract. Laboratory investigations of a turbulent scalar plume are performed to investigate the relationship between instantaneous scalar structure and the resulting mean scalar statistics. A planar laser-induced fluorescence technique is used to image two-dimensional instantaneous spatial plume structure at various locations and in three orthogonal planes. Long image sequences are used to calculate time-averaged scalar statistics (concentration mean, variance and intermittency), and the relationship between these statistics and the observed instantaneous scalar structure is discussed. We present both snapshots and animations of instantaneous scalar structure at various locations within the boundary layer. As with all boundary layer phenomena, the structural variation is greatest in the vertical direction (normal to the bed). The existence of a persistent, relatively uniform layer of dye within the viscous sublayer is identified. In this layer, instantaneous concentrations are moderate, but the persistence of the dye produces a relatively high mean concentration. Above this layer, stronger fluctuations and higher peak concentrations are present, but lower values of the intermittency produce lower mean concentrations. It is argued that a combination of three time-averaged statistics (mean, variance and intermittency) is required to deduce meaningful information about the nature of the instantaneous scalar structure.

PACS numbers: 47.27.-i, 47.27.Nz, 47.27.Te, 47.80.+v

† This paper was chosen from Selected Proceedings of the Second International Symposium on Turbulence and Shear Flow Phenomena (KTH-Stockholm, 27–29 June 2001) ed E Lindborg, A Johansson, J Eaton, J Humphrey, N Kasagi, M Leschziner and M Sommerfeld.

 PII: S1468-5248(02)32522-0 1468-5248/02/000001+24$30.00

JoT 3 (2002) 014

Contents

1. Introduction

Turbulent plumes of scalar quantities (e.g. mass or heat) are ubiquitous in both engineering and nature. The dynamics of systems involving such scalar plumes depend on both the instantaneous and time-averaged (mean) properties of the scalar structure. An understanding of instantaneous processes within a plume is essential for establishing a description of the physics that controls the time-averaged properties. This study examines instantaneous scalar structure at various locations within a turbulent plume, and describes how the characteristics of the instantaneous structure produce several common mean properties of the scalar plume.

Advances in experimental techniques have enabled researchers to obtain scalar data in two or three spatial dimensions as a function of time. The spatial and temporal resolutions of these new techniques have improved to allow a wide range of scalar structures to be accurately resolved. The most common technique is planar laser-induced fluorescence (PLIF) [1]–[7].

We use PLIF to investigate the instantaneous scalar structure of a neutrally buoyant plume in a turbulent boundary layer. The plume source is flush with the bed, and the momentum associated with the scalar release velocity is extremely low. The source geometry is designed to mimic a diffusive odorant release from a source that is buried below a smooth substrate.

Related investigations of plume structure from a variety of different source types have been performed by previous researchers. These include PLIF studies involving neutrally buoyant plumes released from elevated and ground-level sources [7]–[9]. In all of these studies, the source release involves a significant amount of horizontal momentum, and the release is distributed over a large vertical distance (relative to the inner boundary layer scales). A similar investigation performed with a thermal release from a long thin heated wire located at the wall (and other locations) presents only mean temperature results [10]. The present study builds on these previous studies by determining the relationship between the instantaneous scalar structure and resulting time-averaged scalar statistics.

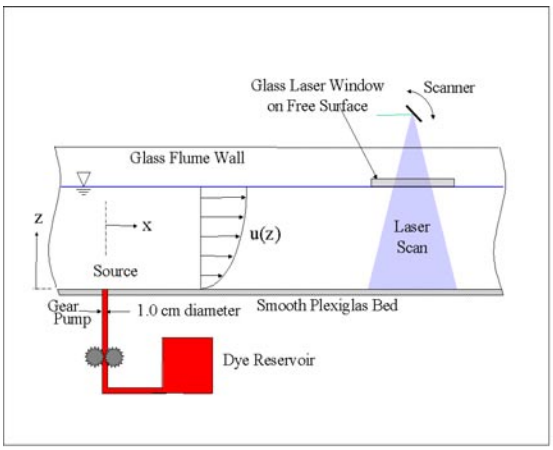

Figure 1. Side view of the flume test section showing the odorant source location and coordinate system (vertical laser scan configuration shown).

2. Experimental procedure

2.1. Flow facility

Plume images were collected in the 3 m test section of an open-channel recirculating flume. The water flow is driven by a digitally controlled pump that fills a 4 m high constant-head tank, allowing for highly constant and repeatable flow conditions. Water from the constant-head tank passes through a diffuser, three homogenizing screens and a two-dimensional contraction before entering a 0.6 m wide rectangular channel section. A 3 mm diameter rod spans the flume floor at the start of the channel, serving as a boundary layer trip. The boundary layer develops over a 2.2 m distance before encountering the plume source at the beginning of the flume test section; the test section continues 3 m downstream from the plume source. The flow depth in the test section is 0.25 m, and the δ_{99} thickness of the momentum boundary layer is 0.10 m. The freestream turbulence levels are approximately 2% of the flow velocity, and flow in the test section is free from artificial secondary flows caused by the diffuser, the contraction, residual pump vorticity etc [11].

The walls of the test section are glass to improve optical clarity. The bed is Plexiglas (painted black to minimize laser reflections), with no roughness elements other than the upstream trip. When the vertical laser sheet is used, a small glass window is placed on the free surface of the flow to eliminate optical refraction caused by the free surface; this window does not alter the flow in the image area. A sketch of the flume test section, along with the odour source and laser sheet (discussed later), is shown in figure 1.

2.2. Odour source design

The odour source is designed to mimic a diffusive-type (i.e. low-momentum) release of a scalar from a flush, bed-level source within a turbulent boundary layer. The odour source is located on the flume centreline, near the upstream edge of the test section (2.2 m downstream of the boundary layer trip). The odour source location is designated $x = 0$. A 20 ppm aqueous solution of the fluorescent dye Rhodamine 6G (Schmidt number = 1250 [12]) is used for the scalar odorant.The dye solution is pumped slowly through a 1 cm diameter circular hole drilled perpendicular to the bed in the floor of the flume. The hole is filled with a

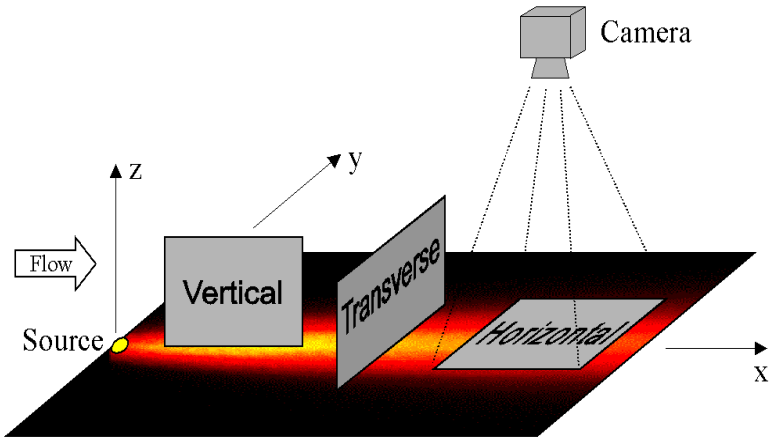

Figure 2. Schematic representation of the orientation of the laser light sheet and resulting image planes used for this study. In the figure, the camera is shown in the position used for 'horizontal' images.

porous foam to provide a uniform flow across the source exit; the foam is mounted flush with the bed of the flume. A small gear pump is used to pump the dye solution through the odour source at a volumetric rate of 3 ml min^{-1}, resulting in a vertical exit velocity of $W_s = 0.063$ cm s^{-1}. The electronic gear pump provides an accurate dose rate with no measurable pulsing.

2.3. Imaging acquisition and processing

Details of the PLIF and image processing techniques used for the present study are given in [6]. A plume of Rhodamine 6G dye is illuminated with a laser light sheet, and the resulting fluorescence field was imaged with a digital camera. In water, Rhodamine 6G has a central excitation (absorption) wavelength of $\lambda_{\text{ex}} = 524$ nm, and a central emission (fluorescence) wavelength of $\lambda_{\text{em}} = 555$ nm [13]. The light sheet was generated by an argon-ion laser with a single-line emission of $\lambda = 514.5$ nm (green) at 1.3 W. In order to decrease the thickness of the light sheet, the laser beam was focused using a lens in conjunction with a beam expander. The focused beam waist diameter for our optical setup was estimated to be 280 μm. The focused laser beam was scanned across the image area using a moving-magnet optical scanner consisting of a square 5 mm mirror actuated by a closed-loop galvanometer. The sweep rate was modulated to correct for laser intensity variations in the direction of the scan [6]. The scanning mirror could be oriented to produce light sheets in the x–z ('vertical'), x–y ('horizontal') and y–z ('transverse') planes, where x, y and z are the streamwise, transverse and vertical directions, respectively. The orientation of these planes is shown schematically in figure 2.

The fluorescence images were acquired using a 1024-by-1024 pixel monochrome digital camera with 12-bit grey scale intensity resolution. A flat-field lens (Micro-Nikkor, $f = 55$ mm) fitted with a narrow-bandpass optical filter (centre wavelength = 557 nm, bandwidth = 45 nm) was used. An image was acquired using the following sequence: (1) the camera began exposing the CCD chip, (2) the optical scanner scanned the focused laser beam across the image area in a single, uni-directional pass, (3) the camera stopped exposing the CCD chip and (4) the optical scanner returned the laser beam to the original stand-by location (just beyond the edge of the image area). A delay was introduced between steps (3) and (4) to allow sufficient time for the camera to shift the image off the chip without exposure contamination from the returning laser beam. All of the steps in the sequence were controlled by analogue and digital signals

Table 1. Experimental flow conditions at $x = 160$ cm.

U_∞ (cm s^{-1})	u_τ (cm s^{-1})	Re_θ
9.84	0.488	540

generated by a computer running a LabView program. The sequence was repeated to produce short image sequences (typically 300 frames) at 15 Hz framing rates, or long sequences (typically 8000 frames) at approximately 3 Hz.

The images captured by the camera contain spatial maps of the fluorescence intensity in the image area. However, the raw data contain unwanted artifacts from the image acquisition system. These artifacts stem from spatial and temporal variations in the laser scan intensity (including those due to quenching), spurious fluorescence from background dye concentrations and nonuniformities in the combined camera/lens system (e.g. pixel response variations, lens vignette). The raw images are therefore post-processed to remove or minimize these errors [6].

2.4. Spatial and temporal resolution

In the plane of the image, the spatial resolution is set by the dimension of the imaged area and the number of pixels in the resulting digital image. In the direction normal to the image plane, the resolution is set by the thickness of the laser sheet (280 μm). The size of the images used in this study is typically about 15 cm $\times$ 15 cm, and the image is mapped onto a 1024×1024 pixel array (the final images presented herein may be cropped, but the resolution remains the same). This results in an in-plane spatial resolution of approximately 150 μm. Thus, each pixel images a cube that with dimensions 150 μm $\times$ 150 μm $\times$ 280 μm. The smallest scalar structures in the flow are set by the Batchelor scale, and can be significantly smaller that the spatial resolution obtained by our system [6]. We could increase the spatial resolution of the system by decreasing our image area. However, we chose the image size based on a compromise between capturing both small scales and the large-scale odorant structure.

The temporal resolution of the image is effectively set by the dynamics of the laser scan (since the timescales of the dye fluorescence and the CCD response are extremely fast [6]). Each image is exposed by a single, uni-directional scan of the laser beam. The total exposure time for the entire pixel array ranged from 8 to 250 ms (depending on the image location), with a typical scan having a duration of 50 ms. A single pixel is exposed for a time approximately equal to 1/1024 of the total scan time across all of the pixels. This small pixel exposure time provides sufficient exposure since all of the available laser power is concentrated in a pixel-scale region at any given point in time. For a 50 ms scan, an individual pixel is exposed for less than 50 μs, during which time a 10 cm s^{-1} flow advects only 5 μm (which is much smaller than the single-pixel image dimension of 150 μm). Thus, local scalar structures are accurately mapped onto the pixel array with a temporal resolution of approximately 50 μs. More details of the spatial and temporal resolution of the imaging system are given by [6].

2.5. Hydrodynamic conditions

Results are presented for a single flow condition with a mean freestream velocity of 9.84 cm s^{-1}, with $Re_\theta = 540$. Flow parameters are summarized in table 1.

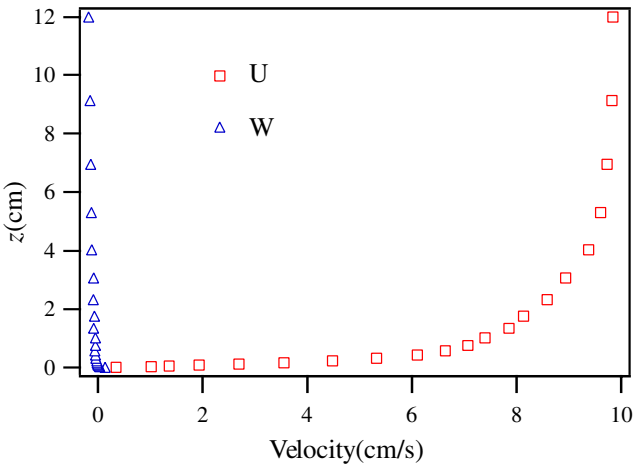

Figure 3. Mean streamwise (U) and vertical (W) velocity profiles measured with a LDA at $x = 160$ cm downstream of the source.

A two-dimensional laser-Doppler anemometer (LDA) was used to record vertical profiles of the mean velocities and turbulence structure. The LDA data were measured at $x = 160$ cm, which is approximately 45 cm further downstream than the location of most of the scalar plume data reported in this paper. However, since the flow has been shown to change very slowly as it passes through the test section [14], these data are good indicators of the flow conditions throughout the test section. Figure 3 shows vertical profiles of the mean streamwise (U) and vertical (W) velocities.

Figure 4 contains measured vertical profiles of normalized turbulence statistics, compared with DNS results (for $Re_\theta = 670$) from Spalart [15]. Streamwise and vertical turbulence intensities $\overline{u^2}$ and $\overline{w^2}$, and the Reynolds stress correlation $\overline{uw}$, are normalized by u_τ^2, the square of the shear velocity. The statistics are plotted versus both the nondimensional wall distance z^+ as well as the dimensional distance z. These data are useful for understanding the hydrodynamic context of the plume images presented later.

3. Mean plume structure

3.1. Concentration

Mean concentration fields in horizontal planes at distances $z = 2$ and 4 cm above the bed are shown in figure 5. The mean concentration has been normalized by the source concentration C_0, and the false colour represents its magnitude, as shown in the legend. Note that the mean concentration is zero near the source ($x = 0$) since mixing has not yet brought the scalar up to the level of the data planes. The mean concentration reaches a peak value on the plume centreline some distance downstream of the source; the distance to this peak increases with distance from the bed. Lateral profiles of normalized mean concentration at several streamwise and vertical locations are shown in figure 6. Each profile is scaled with two parameters: the local centreline concentration C_m, and the plume width σ_y. The parameters are obtained for each profile using a two-parameter least-squares fit to the Gaussian

$$\frac{\overline{C}}{C_\mathrm{m}} = \exp\left(\frac{-y^2}{2\sigma_y^2}\right). \tag{1}$$

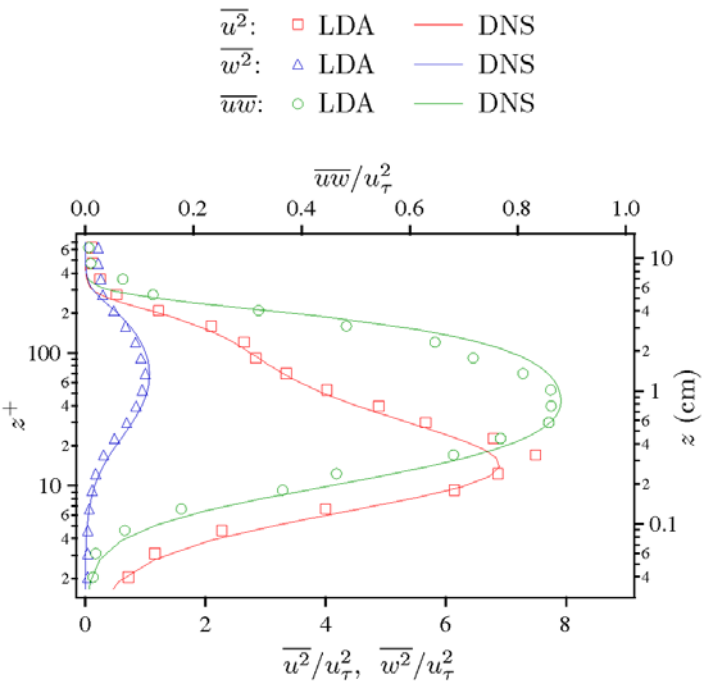

Figure 4. Turbulence intensity and Reynolds stress profiles measured at $x = 160$ cm downstream of the source, including a comparison with DNS results from Spalart [15].

The solid curve in figure 6 is the Gaussian profile given by equation (1). The mean lateral concentration data are clearly Gaussian and self-similar, in agreement with previous experimental studies [8, 9].

The mean concentration field in a vertical plane through the plume centreline is shown in figure 7, where the vertical dimension is exaggerated by a factor of two. Again, the mean concentration is normalized by the source concentration. Strong vertical gradients in the mean concentration are evident, and the aspect ratio (depth over length) of the plume remains relatively thin over the length of the test section.

Finally, the mean normalized concentration field in a vertical plane normal to the flow direction (hereafter referred to as the transverse plane) at $x = 100$ cm is shown in figure 8. Contour lines of mean concentration are approximately elliptical in shape. The higher-concentration contours near the plume axis ($y = 0$, $z = 0$) become compressed in the vertical direction while maintaining a significant lateral extent. This leads to strong vertical gradients of mean concentration near the bed near the plume centreline, whereas the near-bed concentration gradients away from the centreline ($|y| > 4$) are nearly horizontal. We shall demonstrate that the high mean concentrations shown in red in figure 8 result not from high instantaneous concentrations but, instead, from persistent, moderate concentrations in a meandering scalar 'slick' within the viscous wall region.

The mean concentration profiles shown in figures 5, 7 and 8 suggest that the mean plume structure varies slowly in the streamwise (x) direction relative to structural variations in the lateral (y) and vertical (z) directions. As a result, the plume images in the transverse (y–z) plane tend to provide the most information about the mean structural variations. Therefore, we present only transverse images in the following two sections, which address additional measures of mean plume structure (variance and intermittency).

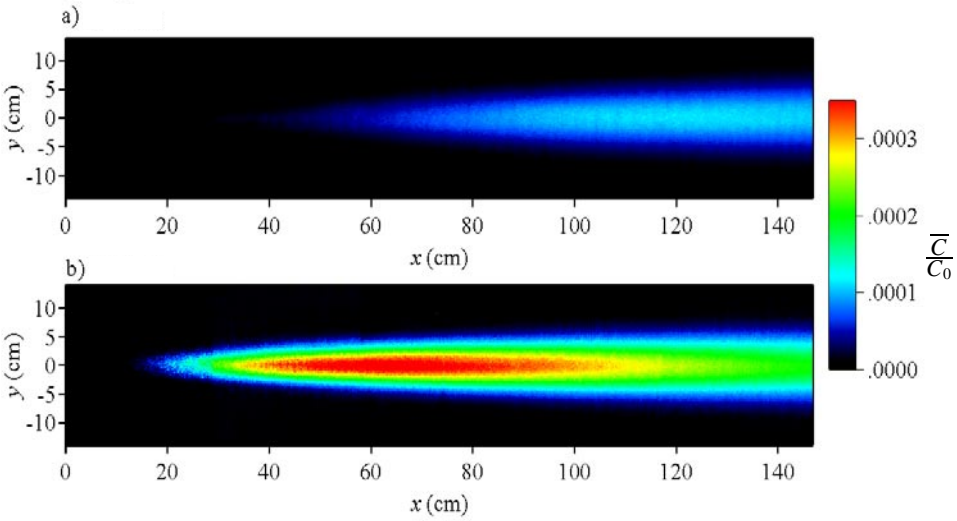

Figure 5. Mean concentration field in horizontal planes at (a) $z = 4$ cm and (b) $z = 2$ cm. Concentrations are normalized by the source concentration C_0 and colour coded as shown in the legend.

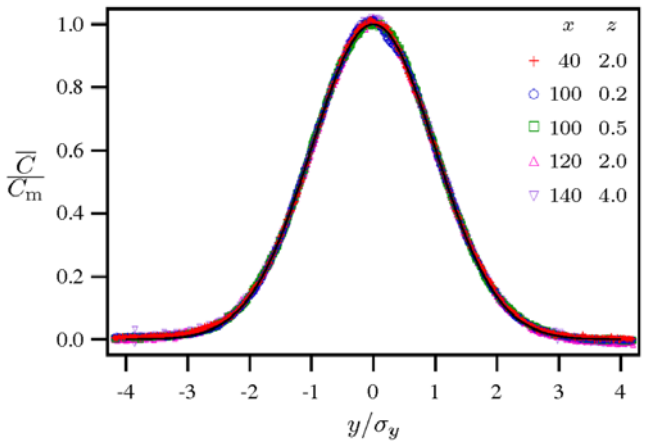

Figure 6. Normalized lateral profiles of mean concentration. The legend gives the location of each profile in units of cm. The solid curve is the Gaussian $\overline{C}/C_{\mathrm{m}} = \exp(-y^2/2\sigma_y^2)$.

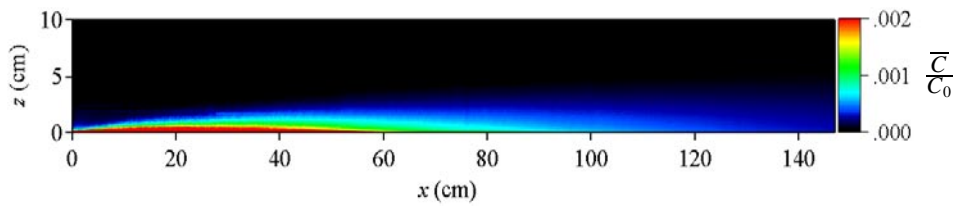

Figure 7. Mean concentration field in a vertical plane along the plume centreline. The vertical dimension is exaggerated by a factor of two. Concentrations are normalized by the source concentration C_0 and colour coded as shown in the legend.

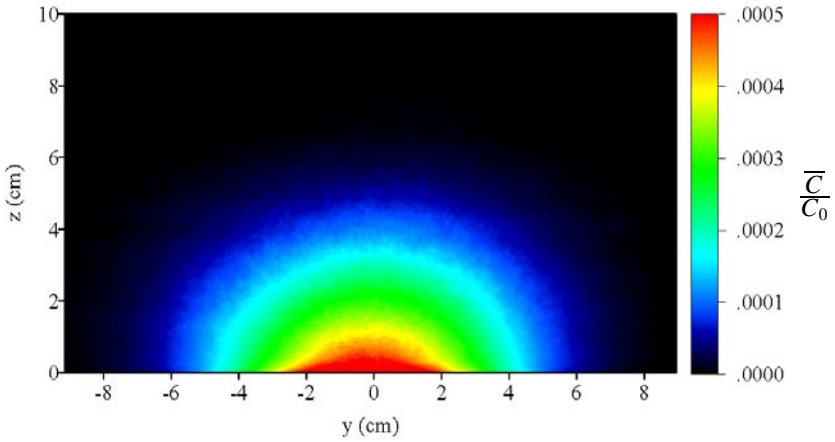

Figure 8. Mean concentration field in a transverse plane normal to the flow at $x = 100$ cm. Concentrations are normalized by the source concentration C_0 and colour coded as shown in the legend.

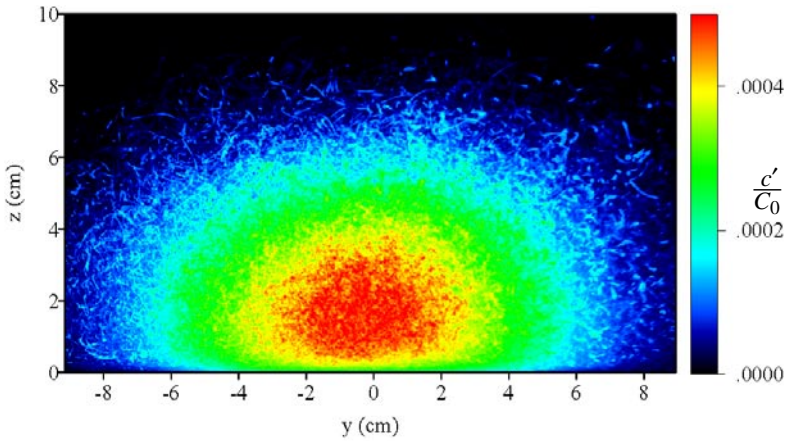

Figure 9. Standard deviation of the concentration field (square root of the variance) in a transverse plane normal to the flow at $x = 100$ cm. The standard deviation is normalized by the source concentration C_0 and colour coded as shown in the legend.

3.2. Variance

A second measure of the time-averaged nature of the plume structure is given by the mean-square concentration variance about the mean, or its square root, the root-mean-square (rms) value of the concentration fluctuations, herein denoted c'. The normalized magnitude of c' in a transverse plane at $x = 100$ cm is shown in figure 9. Note that the fine-scale variations observed in the image are due to incomplete statistical convergence in the image (even with 8000 ensemble averages). Near the periphery of the plume, it is possible to identify discrete scalar structures that were present in only one of the 8000 images used to produce the averaged image.

The spatial structure of c' is significantly different from that of the mean concentration. Whereas the mean concentration peaked either at the bed (close to the plume centreline) or close to the bed (further away from the centreline), the peak value of c' always occurs a significant distance away from the bed. Nonzero values of c' also cover a larger spatial extent than do

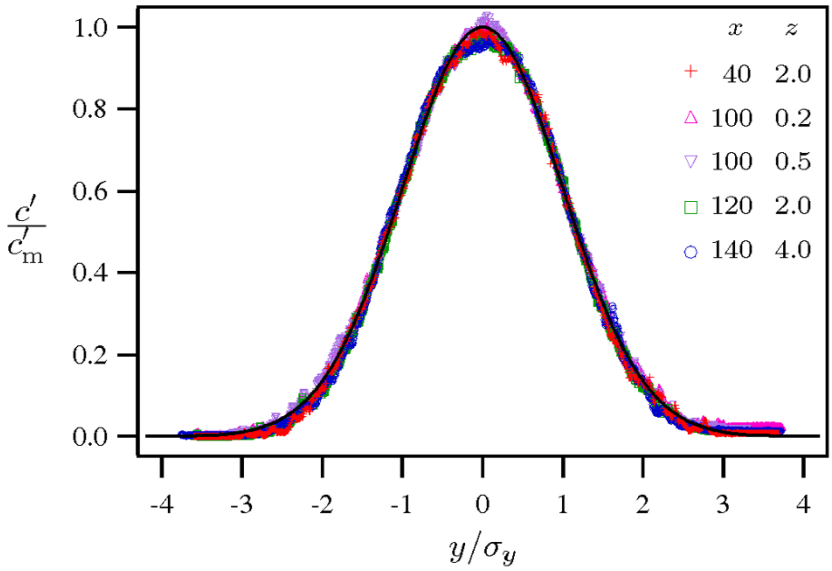

Figure 10. Normalized lateral profiles of rms concentration fluctuation strength. The legend gives the location of each profile in units of cm. The solid line is the Gaussian $c'/c'_m = \exp(-y^2/2\sigma_y^2)$.

values of the mean concentration. That is, infrequent (but strong) concentration structures that occur at the periphery of the plume contribute more significantly to the c' field than they do to the $\overline{C}$ field. Note also that the red region in 8 (corresponding to high mean concentrations) is not accompanied by a region of high c' values in figure 9, and vice versa. This suggests that the red region in figure 8 is associated with persistent moderate concentrations, whereas the red region in figure 9 (which has high c' values, but lower $\overline{C}$ values) is associated with intermittent occurrences of stronger concentration structures.

Although the vertical variation in c' is quite different from that of $\overline{C}$, the lateral variation in the two statistics is similar. Figure 10 shows lateral profiles of c' at several streamwise and vertical locations†. Each profile is scaled with two parameters (c'_m and σ_y) using a two-parameter least-squares fit to a Gaussian equation of the form given by equation (1). The values of σ_y obtained for the c' profiles are larger than those obtained for the corresponding $\overline{C}$ profiles, but the shapes of both sets of profiles are Gaussian.

3.3. Intermittency

The observed differences between the mean ($\overline{C}$) and fluctuating (c') fields can be explained by the concentration intermittency, defined as the percentage of time that the concentration at a point is nonzero (or, more practically, above some threshold value). The intermittency can be calculated as

$$\gamma = \text{prob}\,[C \geq C_T] \tag{2}$$

where C_T is a concentration threshold value; the choice of this parameter is somewhat arbitrary [16]. For the results presented here, we have chosen $C_T = 0.0002C_0$, which is small

† The lateral profiles shown in figures 6 and 10 were calculated from images taken in the x–y plane. The lateral profiles could then be averaged over a short distance (typically 1 cm) in the streamwise direction. The streamwise averaging distance was always small relative to the streamwise distance over which $\overline{C}$ or c' varied.

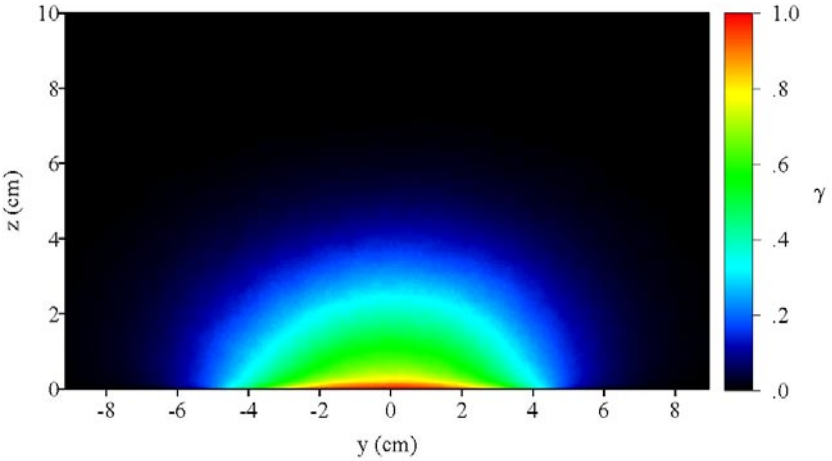

Figure 11. Intermittency of the concentration field in a transverse plane normal to the flow at $x = 100$ cm.

compared with C_0 yet large compared with the experimental noise levels [6]. Note that the definition of 'intermittency' is counter-intuitive: *a steady signal has a high intermittency, and a sporadic signal has a low intermittency.*

Figure 11 shows values of the concentration intermittency in a transverse plane at $x = 100$ cm. The presence of nonzero concentration is most persistent in a very thin near-bed layer shown in red in the figure ($\gamma \approx 1$ in this layer). The thickness of this layer is approximately 0.1 cm, or about 5 viscous wall units, corresponding to the thickness of the viscous sublayer (VSL) [17]. The turbulence intensities and Reynolds stresses in the VSL ($z^+ < 5$) are near zero (see figure 4). The relatively low level of fluid exchange between the VSL and the rest of the flow leads to 'trapping' of dye. During the experiments, dye would persist within the VSL for a minute or so after the dye source pump was stopped. Dye above the VSL would quickly advect downstream, while dye within the VSL remained trapped within the viscous, slow-moving layer. Although turbulent mixing within the VSL is minimal, the effect of shear dispersion from the strong near-wall velocity gradient is significant. The shear dispersion minimizes any spatial or temporal structure within the VSL, resulting in the low near-bed values of c' seen in figure 9.

Scalar trapping within the VSL results in intermittency behaviour that varies strongly with distance from the bed. Lateral profiles of γ from the data in figure 11 at $x = 100$ cm are shown in figure 12. Far from the bed ($z = 2$ cm), the lateral profile of γ is Gaussian, with a maximum value of 0.4 on the plume centreline. That is, dye with concentration $C \geq C_T$ is present at this location 40% of the time. Away from the plume centreline, $\gamma \to 0$ in a Gaussian fashion. Closer to the bed, two things happen: the peak centreline value of γ increases towards unity, and the shape of the distribution becomes non-Gaussian. Specifically, the profile at $z = 0.01$ cm ($z^+ = 0.5$) has a large region around the plume centreline where the value of γ is unity, meaning that dye is always present. The deviation of the γ profiles from Gaussian is further demonstrated in figure 13. The figure contains the $z = 2$ and 0.01 cm profiles from figure 12, with the magnitude of the profiles normalized by their centreline values. The $z = 2$ cm profile is Gaussian, shown by the Gaussian fit to the profile (black dotted curve). The $z = 0.01$ cm profile is clearly non-Gaussian. The small kurtosis of the near-wall intermittency profiles results from the constraint that $0 \leq \gamma \leq 1$; pdfs of intermittency values near the wall are clipped on the $\gamma = 1$ side of the distribution.

The spatial behaviour of the time-averaged statistics of concentration, variance and intermittency results from the statistical nature of the instantaneous scalar structures at

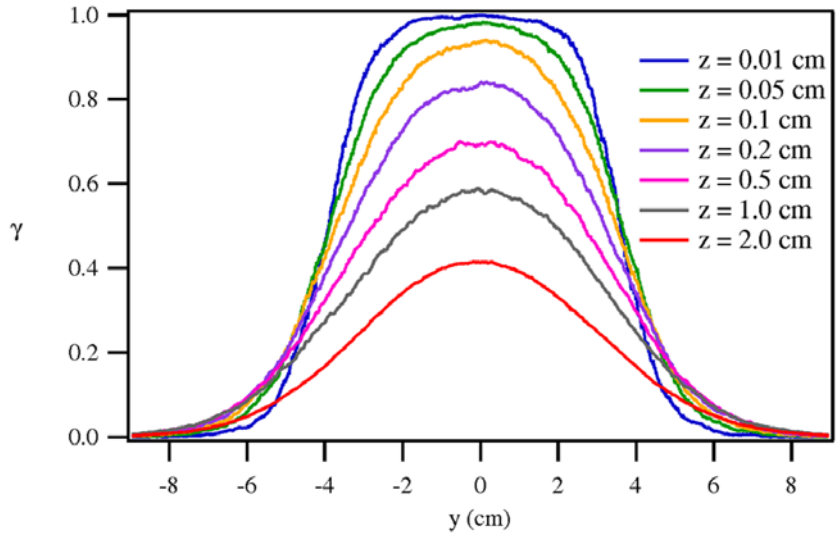

Figure 12. Lateral profiles of concentration intermittency at $x = 100$ cm.

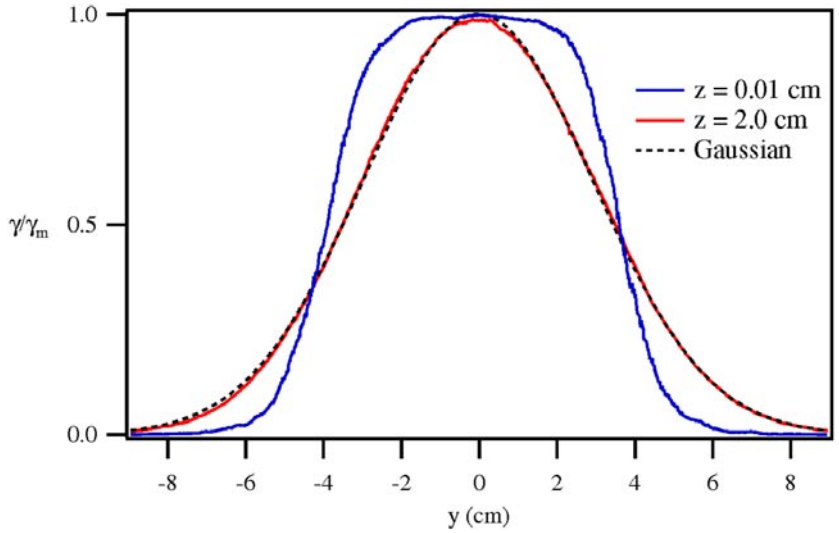

Figure 13. Normalized lateral profiles of concentration intermittency at $x = 100$ cm. The black dotted curve is a Gaussian fit to the $z = 2.0$ cm profile.

different locations within the flow. In the next section, we show representative snapshots of the instantaneous scalar structure in different locations and in different planes. We then discuss how the nature of the instantaneous structures leads to the observed time-averaged statistics.

4. Instantaneous plume structure

An examination of the instantaneous scalar structure at various locations within the plume leads to a better understanding of the processes that produce the time-averaged statistics presented in the previous section. Choosing a single snapshot of instantaneous structure at a given location is challenging, however, due to extreme variability between individual frames in a time sequence of images. To mitigate this challenge, we present instantaneous scalar structure data in two formats:

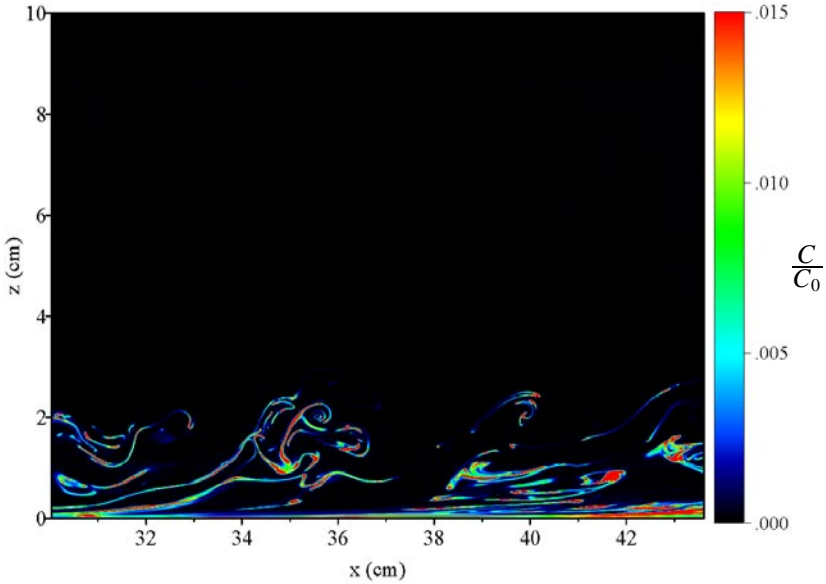

Figure 14. Instantaneous scalar structure in a vertical plane through the plume centreline in a streamwise reach near $x = 30$ cm.

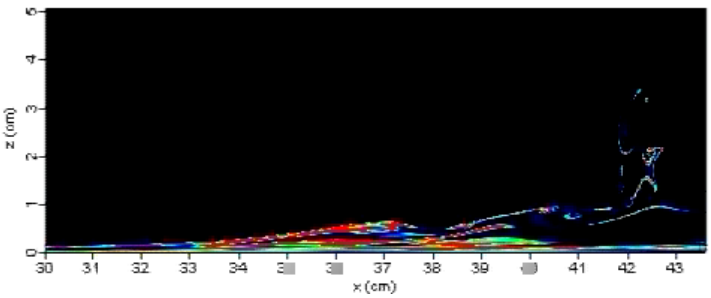

Figure 15. Animation of scalar structure in a vertical plane through the plume centreline in a streamwise reach near $x = 30$ cm.

high-resolution single-frame snapshots, accompanied by low-resolution animations from the same location. Low resolution is required for the animations to conform with restrictions on file size. For the single-frame snapshots, we have endeavoured to present images that are representative of typical local instantaneous structure. The animations are then useful to provide information about the temporal variation in the structure seen in the snapshots. Note that the colour-scale generally changes between the images which follow to accommodate the change in concentrations at different locations. The normalized concentrations associated with each colour in a particular image are shown in that image's legend.

4.1. Vertical plane

We begin by presenting a set of images of the instantaneous scalar structure in a vertical (x–z) plane at four locations within the flow, each spanning a region 10 cm high and 14 cm in the flow direction. Figure 14 contains an image of the instantaneous scalar structure in a vertical plane on the plume centreline ($y = 0$) in a streamwise reach starting at $x = 30$ cm. The most striking feature in this image is the strongly filamentous nature of the scalar structures. The

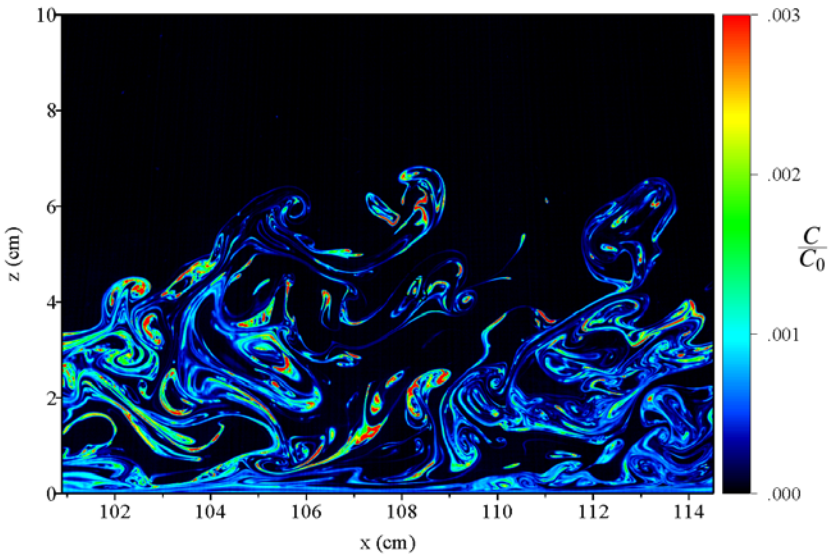

Figure 16. Instantaneous scalar structure in a vertical plane through the plume centreline in a streamwise reach near $x = 100$ cm.

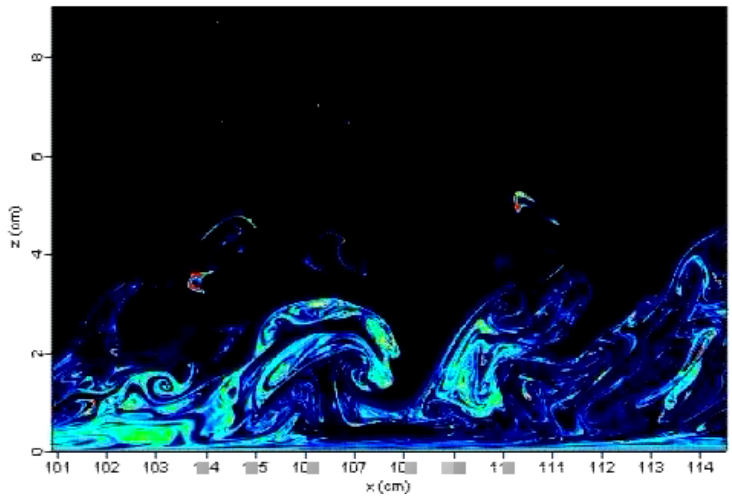

Figure 17. Animation of scalar structure in a vertical plane through the plume centreline in a streamwise reach near $x = 100$ cm.

image is from a location relatively close to the source, and very little molecular diffusion (mixing) of the filaments is evident. Instead, the filaments are being stretched and strained (stirred) by the action of the turbulence. Within the filaments, the dye concentration is quite strong and uniform; outside the filaments, the concentration is effectively zero. The dye structures generally do not spread very far above the bed, but those that do appear to be linked back to the bed. Close inspection of the figure reveals a continuous layer of dye within the VSL ($z < 0.1$ cm). It appears that the dye trapped within the VSL acts as a reservoir of dye for large-scale turbulent bursts. The rising structure of dye in the region between $x = 34$ and 36 cm is an example of a burst structure that is lifting dye away from the VSL. Sweeping motions of dye-free (black) fluid are clearly evident immediately upstream and downstream of the burst. An animation of the temporal change in the scalar structure in the same location as figure 14 is shown in figure 15.

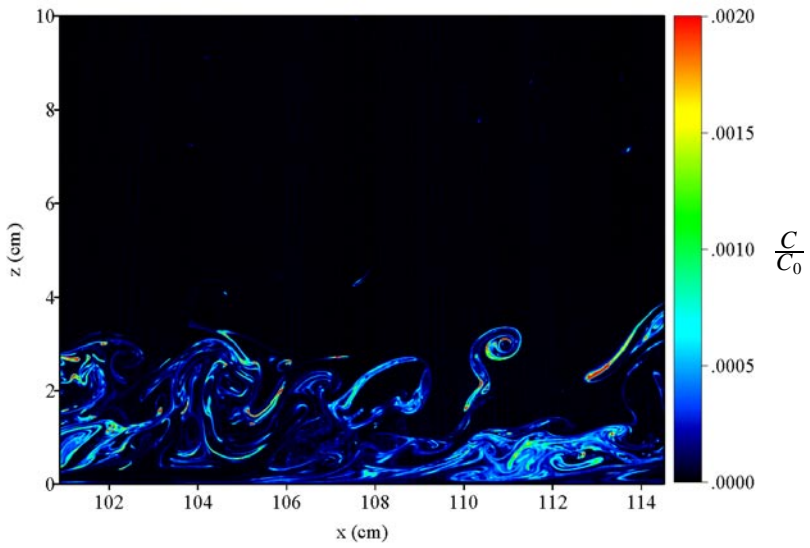

Figure 18. Instantaneous scalar structure in a vertical plane with a 5 cm lateral offset from the plume centreline.

The animation reveals that the burst-driven pattern of vertical dye migration is ubiquitous.

Figure 16 is another snapshot in a vertical plane on the plume centreline, this one located farther downstream than figure 14, at a streamwise reach starting at $x = 100$ cm. The scalar structures now protrude much farther away from the wall, although the same pattern of bursting structures linked back to the wall is evident. Many of the scalar filaments are still extremely thin, due to three-dimensional turbulent straining which acts to elongate coherent structures. However, a wider range of concentration magnitudes is visible in this image, as mixing begins to dilute local structures. The continuous layer of dye within the VSL is still clearly visible, although the concentration has decreased relative to the upstream image. By comparing figure 16 with the images of time-averaged statistics in the transverse plane in figures 8, 9 and 11, the processes that produce the mean statistics become clear. For example, the mean concentrations in figure 8 rise to a maximum value at the bed. The instantaneous structure visible in figure 16, shows that these high mean concentrations result not from high instantaneous concentrations, but from extremely persistent (high-γ) near-bed structures with quite moderate concentration values. In fact, the strongest concentration structures tend to occur as highly localized patches within a vertical band between $z = 1$ and 4 cm ($45 < z^+ < 180$). These strong fluctuating concentration structures produce the high values of c' in the same vertical band (as seen in figure 9), but they do not contribute to a high mean concentration because the scalar structures in this band are very intermittent (as seen in figure 11). Away from the wall (e.g. $z > 1$ cm), the mean concentration is driven largely by the magnitude of the intermittency, since the range of concentration values in this region is relatively constant with depth. For example, the mean concentration at $z = 7$ cm is near zero not because instantaneous concentrations there are small (in fact, when they do occur, they are large), but because they tend to occur there so infrequently. When concentration structures *do* exist at $z = 7$ cm, they appear to have been advected away from the wall by episodic, large-scale coherent turbulent eddies. Once a dye filament is transported this far away from the wall, it tends to persist in a well defined, high-concentration structure due to the low local turbulence intensities (see figure 4). An animation of the temporal change in the scalar structure in the same location as figure 16 is shown in figure 17.

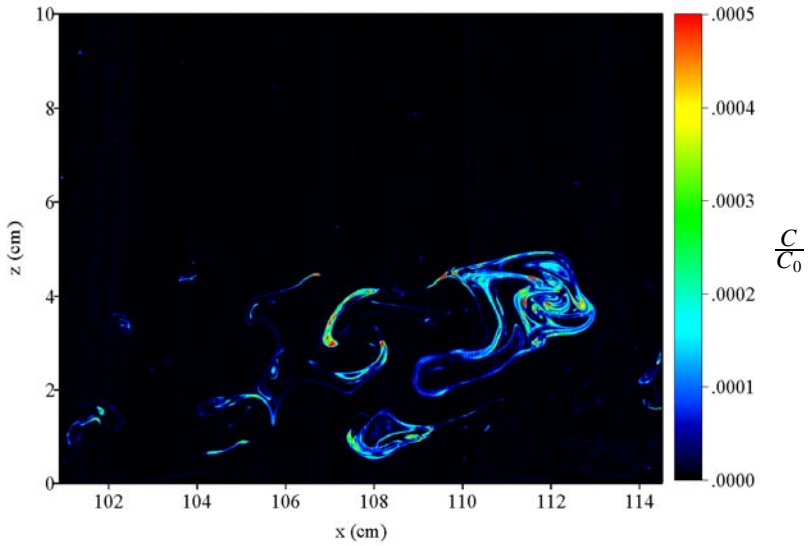

Figure 19. Instantaneous scalar structure in a vertical plane with a 8 cm lateral offset from the plume centreline.

Figures 18 and 19 are vertical images taken at the same streamwise location as figure 16, but at lateral distances away from the plume centreline ($y = 5$ and 8 cm, respectively). In figure 18, two features are evident: the dye structures do not extend as far away from the wall, and the trapped dye within the VSL is less persistent than at the plume centreline. Further away from the centreline (figure 19), the near-bed scalar structures are completely absent. The thin film of dye-laden fluid within the VSL does not extend far from the plume centreline due to the highly viscous nature of the flow near the bed. Turbulent burst structures, however, *do* advect dye filaments vertically from the VSL. Once these filaments move away from the wall, larger lateral turbulent eddies (whose near-wall sizes are constrained) can episodically transport dye towards the plume periphery. This lateral transport tends to be concentrated in a vertical band that does not extend all the way to the bed (due to the aforementioned processes) nor too far away from the bed (since its transport relies on a combination of two episodic events; a large vertical structure and a large lateral structure). The resulting off-axis instantaneous structure consists of coherent, strong filaments that occur with diminishing frequency away from the axis. The resulting low $\overline{C}$, high c' and low γ values at $y = 5$ cm over an intermediate range of depths is evident in figures 8, 9 and 11.

4.2. Transverse plane

A different perspective can be obtained by looking at the instantaneous concentration structures in a transverse (y–z) plane. Figure 20 is a transverse image at $x = 40$ cm (within the streamwise reach shown in figure 14), with an accompanying animation from the same location given in figure 21. Figure 22 is a transverse image further downstream at $x = 100$ cm (within the streamwise reach shown in figures 16–19). An animation corresponding to the location shown in figure 22 is given in figure 23. The transverse images reveal the trapped dye within the VSL; the dye is concentrated and narrowly confined in figure 20, with weaker concentrations but a broader lateral extent in figure 22. The included animations corresponding to the images in figures 20 and 22 show the trapped dye within the VSL slowly sloshing from side to side

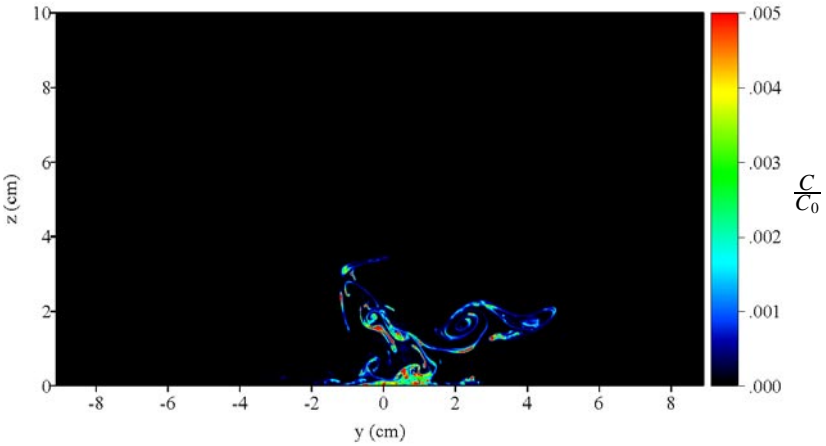

Figure 20. Instantaneous scalar structure in a transverse plane at $x = 40$ cm.

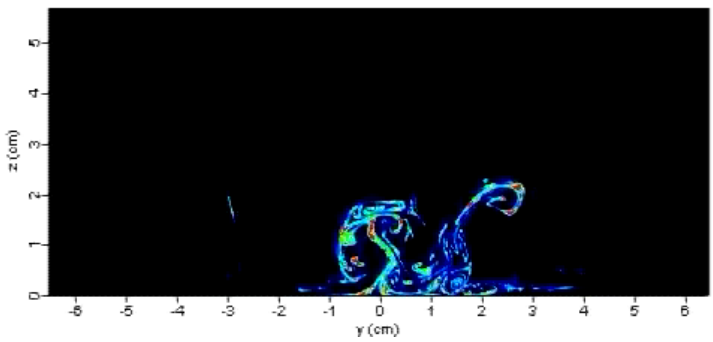

Figure 21. Animation of scalar structure in a transverse plane at $x = 40$ cm.

in response to pressure fluctuations from the outer flow. These animations further illustrate coherent momentum structures lifting dye filaments from the VSL reservoir. Once removed from the bed, episodic lateral motions spread dye away from the axis. The transverse images reveal the presence of coherent, large-scale streamwise vortex structures in the momentum field that wrap scalar filaments into spiral patterns. The animations (figures 21 and 23) show that these vortex structures persist within the frame for significant periods of time, indicating a correspondingly long coherence length scale in the streamwise direction.

4.3. Horizontal plane

The vertical variation in instantaneous scalar structure can be best observed by comparing horizontal slices through the plume at differing heights. A horizontal image spanning a lateral and streamwise range reveals the spatial patterns at a given vertical location. Figures 24 and 25 contain four horizontal images from a single streamwise reach near $x = 100$ cm; each consecutive image is located closer to the bed.

Figure 24(top) is the farthest from the bed, at $z = 4$ cm. The intermittency at this vertical location is generally less than 0.2; dye typically reaches this location in conjunction with large-scale coherent vertical motions. As discussed earlier, the scalar structures that do occur at this vertical location tend to persist relatively unchanged as they advect downstream due to the low turbulence intensities. Note that, in general, individual scalar structures are not interconnected

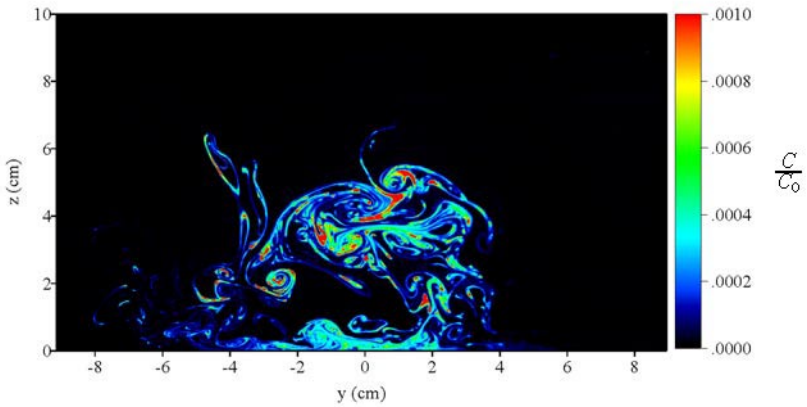

Figure 22. Instantaneous scalar structure in a transverse plane at $x = 100$ cm.

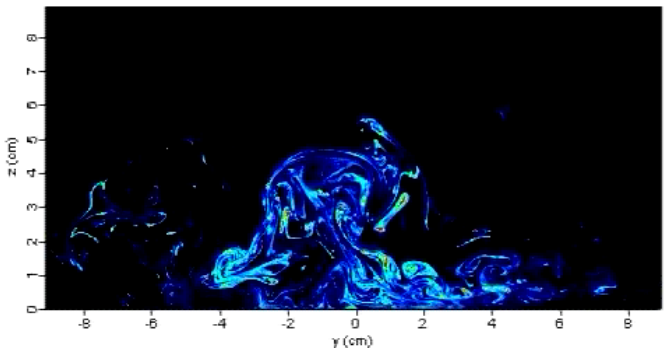

Figure 23. Animation of scalar structure in a transverse plane at $x = 100$ cm.

within the horizontal plane. However, the individual structures generally maintain a degree of coherency in the direction towards the bed (compare with figure 16). Figure 24(bottom) is a similar image, at $z = 2$ cm (figures 24(top) and 24(bottom) share the same colour scale). The intermittency at this location is clearly higher, and a more continuous range of concentrations is present (due to higher levels of turbulent mixing). The peak concentrations at $z = 2$ cm are not noticeably stronger than at $z = 4$ cm, but they occur more frequently (along with all other concentration levels), leading to a high mean concentration.

While the two images in figure 24 are in the outer layer of the momentum boundary layer, the two images in figure 25 are located closer to the bed, in the inner layer. Figures 25(top) and 25(bottom) share the same colour scale, but the scale differs from that used in the previous figures. Figure 25(top) is at $z = 0.5$ cm ($z^+ = 25$), and figure 25(bottom) is at $z = 0.2$ cm ($z^+ = 10$). The increased effects of shear, streamwise turbulence intensity and viscosity become evident at these lower levels. As the distance from the bed decreases, the intermittency rises dramatically, but the diversity of concentration magnitudes drops concurrently. The strong shear and turbulence act to smear out well defined concentration structures into blurred structures with lower concentrations. Again, the mean concentration is seen to be rising due to increasing values of the intermittency, rather than to increasing concentrations. Of particular note in figure 25(bottom) is the streaky nature of the scalar structure in the streamwise direction. This behaviour is associated with the well known streaks in the structure of the momentum field within the VSL.

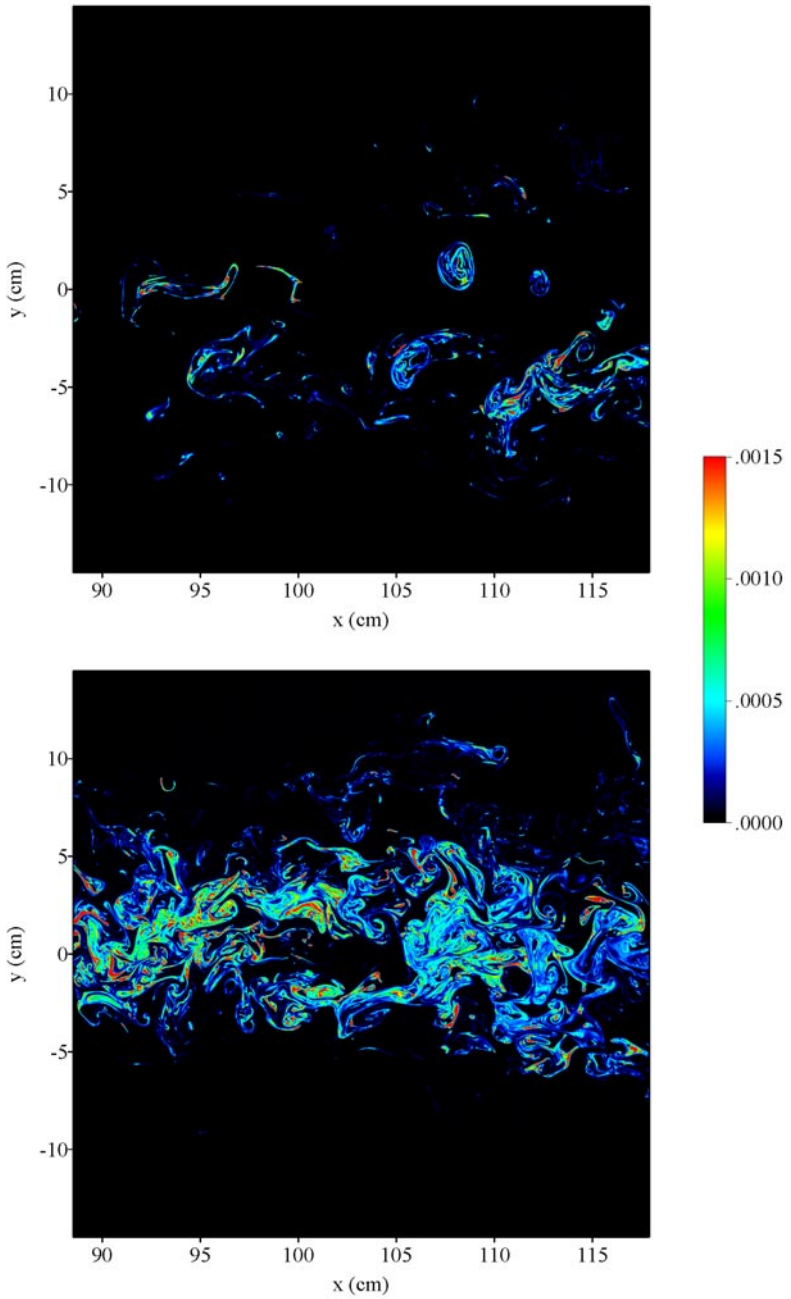

Figure 24. Instantaneous scalar structure in a horizontal plane in a streamwise reach near $x = 100$ cm. The vertical distance of the plane from the bed is (top) $z = 4$ cm and (bottom) $z = 2$ cm.

Animated sequences corresponding to figures 25(top) and 25(bottom) are given in figures 26(top) and 26(bottom). These two animations clearly show how the scalar structure changes as the distance to the bed decreases. In particular, figure 26(bottom) (located at $z = 0.2$ cm, or $z^+ = 10$) shows the temporal evolution of viscous streaks. Of particular interest is the streamwise coherency associated with the streaks. The animation also exemplifies the persistence of near-bed dye that results in high near-bed intermittencies.

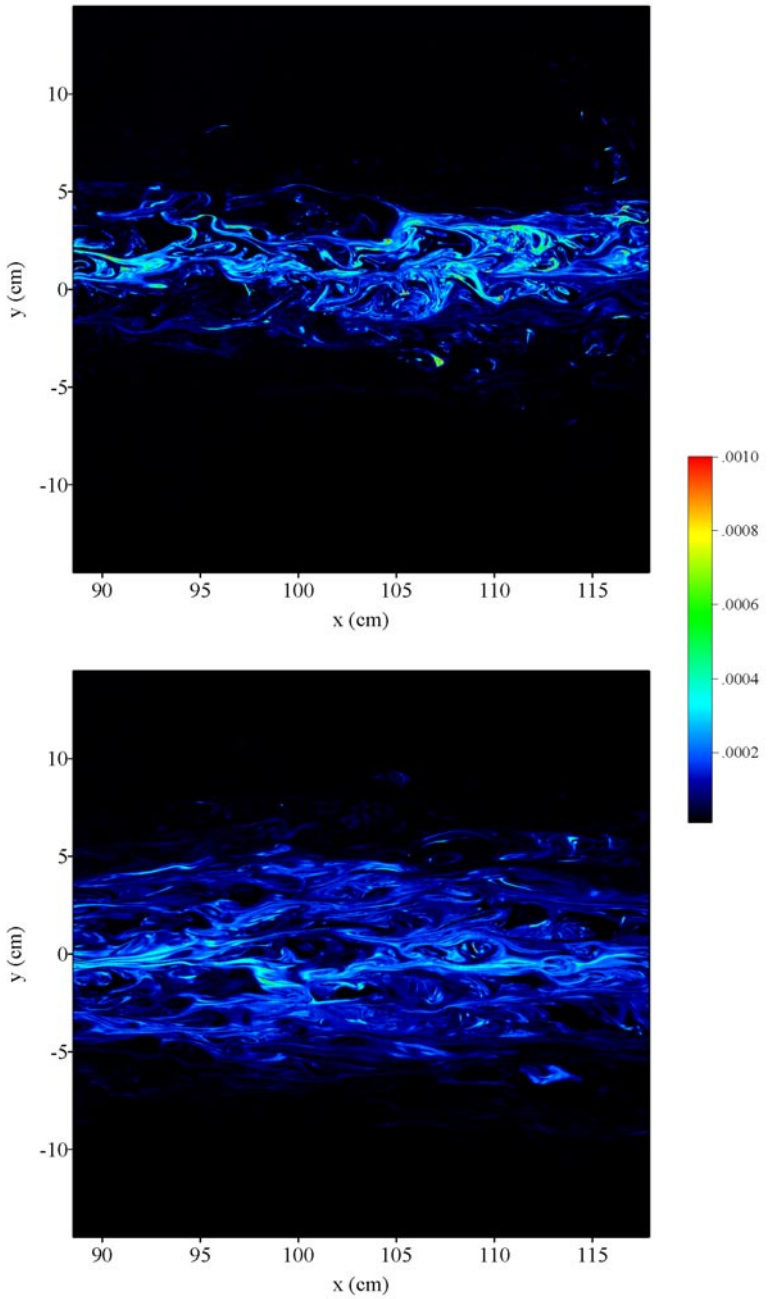

Figure 25. Instantaneous scalar structure in a horizontal plane in a streamwise reach near $x = 100$ cm. The vertical distance of the plane from the bed is (top) $z = 0.5$ cm and (bottom) $z = 0.2$ cm.

The changes in the structure of the scalar field at different distances from the bed can be examined quantitatively by looking at probability density functions (pdfs) of the scalar field. The turbulent scalar field is known to exhibit small-scale (internal) intermittency characterized by strong variability in the scalar dissipation ϵ_θ [18]. The statistics of ϵ_θ and hence of $\partial\theta/\partial t$ (which is often used as a surrogate for quantifying ϵ_θ) are therefore non-Gaussian. To investigate the statistics of $\partial\theta/\partial t$, we calculated the normalized scalar difference $\Delta\theta(r)/\Delta\theta'(r)$, where $\Delta\theta(r) =$

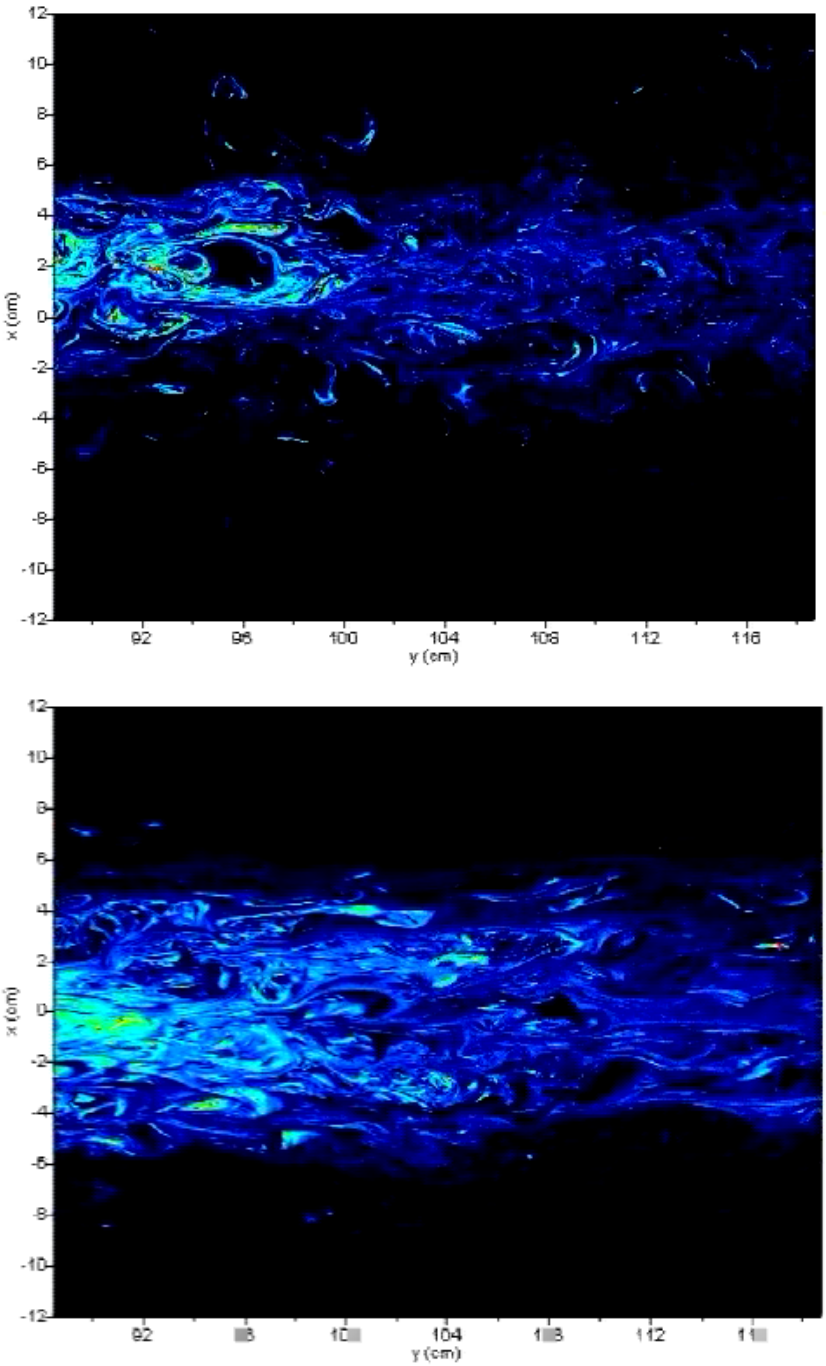

Figure 26. Animations of scalar structure in a horizontal plane in a streamwise reach near $x = 100$ cm. The vertical distance of the plane from the bed is (top) $z = 0.5$ cm and (bottom) $z = 0.2$ cm.

$\theta(r) - \theta(0)$, r is a streamwise spatial separation and $\Delta\theta' = \langle \Delta\theta^2 \rangle^{\frac{1}{2}}$. In figure 27, we plot the pdf of the normalized scalar differences for a separation difference $r = \mathcal{L}_\theta$ where $\mathcal{L}_\theta$ is the local scalar integral scale. Values for $\mathcal{L}_\theta$ were calculated by integrating the scalar autocorrelation function using long, 2000 Hz scalar records acquired with a single-point LIF probe [6]. Figure 27 contains pdfs calculated at three different vertical locations ($z = 4$, 2 and 0.5 cm, corresponding to

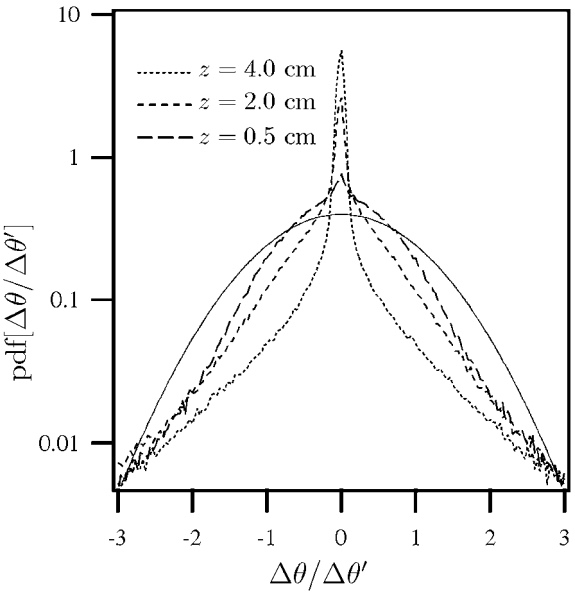

Figure 27. The pdf of the normalized scalar difference at a horizontal separation distance $r = \mathcal{L}_\theta$ for three vertical locations in the boundary layer. All statistics were calculated at $x = 100$ cm. A Gaussian is shown (solid curve) for comparison.

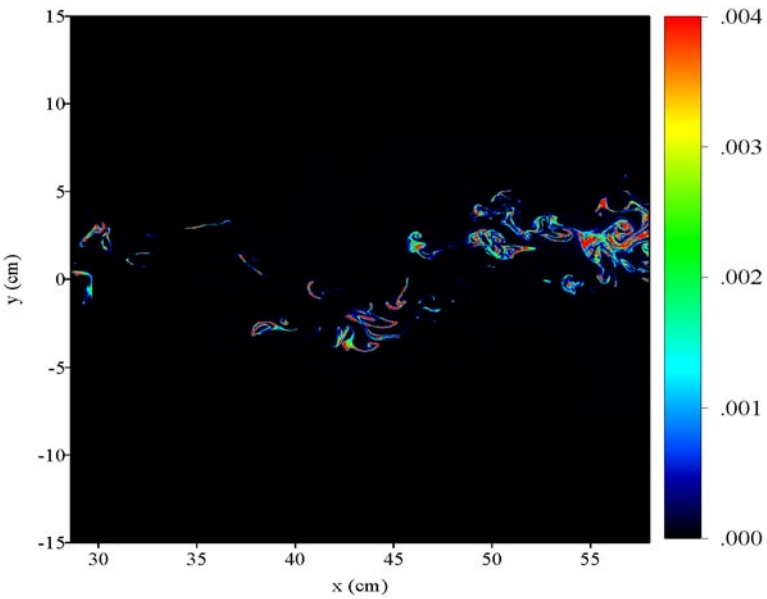

Figure 28. Instantaneous scalar structure in a horizontal plane in a streamwise reach near $x = 30$ cm, at $z = 2$ cm.

figures 24(top), 24(bottom) and 25(top), respectively). A Gaussian is also shown as a solid curve in the figure for reference. The scalar difference is strongly non-Gaussian at all vertical locations in the flow, but most strongly at locations away from the bed where the intermittency is largest.

The nature of the scalar structure observed at a given distance from the bed depends on two factors: the nature of the momentum field at that height (as previously discussed), and the

streamwise distance from the source. The latter dependence results from the plume's vertical development as it advects in the streamwise direction. Figure 28 shows the instantaneous scalar structure at $z = 2$ cm (same as figure 24(bottom)) at an upstream reach near $x = 30$ cm. The upstream scalar structure at $z = 2$ cm is qualitatively comparable to the downstream scalar structure higher up at $z = 4$ cm (figure 24(top)). This vertical development is a feature of the developing scalar field, independent of growth of the momentum field. However, other features of the scalar structure are directly tied to the local development of the momentum field. In particular, the vertical extent of the near-wall scalar structure is governed by the streamwise development of the VSL, which is a feature of the momentum field, independent of the scalar field.

5. Conclusions

This study quantifies the spatial development of basic statistics in a scalar plume developing within a turbulent boundary layer. The focus of the study is to explain the time-averaged statistical behaviour of the plume in the context of local instantaneous scalar structure. Since the scalar in this study is released at the bed with near-zero vertical momentum, the vertical scalar flux is controlled entirely by mixing caused by the momentum boundary layer. The VSL is seen to act as a scalar reservoir through a process of scalar trapping. This reservoir serves as a source for vertical scalar flux at downstream locations through turbulent mixing processes. Once the scalar is elevated into the flow, it can undergo large vertical or lateral motions due to coherent structures in the velocity field.

As with most boundary layer phenomena, the strongest spatial variations in the scalar plume structure occur in the vertical direction. Close to the bed, the scalar field is highly persistent (high γ), with concentration magnitudes that are moderate and narrow banded. The concentration structures in this region are strongly mixed by the shear and high turbulence intensities. The time-averaged result is a high mean concentration with low variance. Far from the bed, scalar structures are highly intermittent, but typically contain strong peak concentrations. These scalar structures persist in time and space due to low shear and turbulence levels. The time-averaged result is a low mean concentration, with high concentration variance.

The nature of the instantaneous scalar structure at a given location cannot be described with a single time-averaged statistic. For example, a low value of $\overline{C}$ does not imply that the local concentration peaks are small, or vice versa. In fact, the opposite is often true. However, the combination of the three time-averaged statistics of $\overline{C}$, c' and γ provides a meaningful measure of the instantaneous scalar characteristics.

Acknowledgments

This work was supported by the Office of Naval Research's Chemical Plume Tracing Program, under grants N00014-97-1-0706, N00014-98-1-0785 (Koseff) and N00014-00-1-0794 (Crimaldi).

References

[1] Koochesfahani M M and Dimotakis P E 1985 Laser-induced fluorescence measurements of mixed fluid concentration in a liquid plane shear layer *AIAA J.* **23** 1700–7

[2] Brungart T A, Petrie H L, Harbison W L and Merkle C L 1991 A fluorescence technique for measurement of slot injected fluid concentration profiles in a turbulent boundary layer *Exp. Fluids* **11** 9–16

[3] Dahm W J A, Southerland K B and Buch K A 1991 Direct, high resolution, four-dimensional measurements of the fine scale structure of Sc $\gg$ 1 molecular mixing in turbulent flows *Phys. Fluids* A **3** 1115–27

[4] Ferrier A J, Funk D R and Roberts P J W 1993 Application of optical techniques to the study of plumes in stratified fluids *Dyn. Atmos. Oceans* **20** 155–83

[5] Houcine I, Vivier H, Plasari E and Villermaux J 1996 Planar laser induced fluorescence technique for measurements of concentration in continuous stirred tank reactors *Exp. Fluids* **22** 95–102

[6] Crimaldi J P and Koseff J R 2001 High-resolution measurements of the spatial and temporal structure of a turbulent plume *Exp. Fluids* **31** 90–102
[7] Webster D R and Weissburg M J 2001 Chemosensory guidance cues in a turbulent chemical odor plume *Limnol. Oceanogr.* **46** 1034–47
[8] Fackrell J E and Robins A G 1982 Concentration fluctuations and fluxes in plumes from point sources in a turbulent boundary layer *J. Fluid Mech.* **117** 1–26
[9] Bara B M, Wilson D J and Zelt B W 1992 Concentration fluctutation profiles from a water channel simulation of a ground-level release *Atmos. Environ.* A **26** 1053–62
[10] Shlien D J and Corrsin S 1976 Dispersion measurements in a turbulent boundary layer *Int. J. Heat Mass Transfer* **19** 285–95
[11] Crimaldi J P 1998 Turbulence structure of velocity and scalar fields over a bed of model bivalves *PhD Thesis* Stanford University
[12] Barrett T K 1989 Nonintrusive optical measurements of turbulence and mixing in a stably-stratified fluid *PhD Thesis* University of California, San Diego
[13] Penzkofer A and Leupacher W 1987 Fluorescence behaviour of highly concentrated rhodamine 6g solutions *J. Lumin.* **37** 61–72
[14] O'Riordan C A, Monismith S G and Koseff J R 1993 A study of concentration boundary-layer formation over a bed of model bivalves *Limnol. Oceanogr.* **38** 1712–29
[15] Spalart P R 1988 Direct simulation of a turbulent boundary layer up to $\mathrm{Re}_{\delta_2} = 1410$ *J. Fluid Mech.* **187** 61–98
[16] Chatwin P C and Paul J Sullivan 1989 The intermittency factor of scalars in turbulence *Phys. Fluids* A **4** 761–63
[17] Tennekes H and Lumley J L 1972 *A First Course in Turbulence* (Cambridge, MA: MIT Press)
[18] Warhaft Z 2000 Passive scalars in turbulent flows *Annu. Rev. Fluid Mech.* **32** 203–40